IOP Publishing Measurement Science and Technology
Meas. Sci. Technol. **32** (2021) 055007 (13pp) https://doi.org/10.1088/1361-6501/abd81e

Powder thermal conductivity measurements in laser powder-bed fusion: an uncertainty study with sensitivity analysis

Shanshan Zhang[1], **Brandon Lane**[2] **and Kevin Chou**[1]

[1] Department of Industrial Engineering, University of Louisville, Louisville, KY 40292, United States of America
[2] Engineering Laboratory, National Institute of Standards and Technology, Gaithersburg, MD 20899, United States of America

E-mail: shanshan.zhang@utrgv.edu

Received 11 October 2020, revised 10 December 2020
Accepted for publication 4 January 2021
Published 25 March 2021

Abstract

Laser flash testing and finite element (FE) heat transfer simulations have been together applied to measure the thermal conductivity of metallic powder contained in a solid specimen made by laser powder bed fusion (L-PBF) additive manufacturing. However, input parameters to the FE model potentially influence the accuracy of thermal conductivity evaluations. This study intends to investigate the effect of major uncertainties in the measurement of metallic powder thermal conductivity in L-PBF, including specimen dimensions, solid material properties, as well as the irradiation area and pyrometer detected area in laser flash testing, and to determine the sensitivity of various factors. A dummy-treated Taguchi method with different levels of the studied factors was utilized using the FE simulations and an inverse method. The results show that the dimension of the specimen's internal powder-enclosed cavity and the solid material properties have dominant effects on the evaluation of powder thermal conductivity. In addition, predictions from the regression equations are verified and give a reasonable agreement with the simulated powder thermal conductivity values.

Keywords: sensitivity analysis, laser powder bed fusion, laser flash, finite element modeling, inverse method, powder thermal conductivity, Taguchi method

(Some figures may appear in colour only in the online journal)

1. Introduction

In recent decades, laser powder bed fusion (L-PBF) additive manufacturing (AM) has been employed in multiple engineering applications due to its irreplaceable advantages, such as a finer surface and better part quality compared to other metal AM technologies [1, 2]. Such a process applies a laser heat source on the top of the metal powder bed along the model profile layer by layer, to fabricate a three-dimensional (3D) object. During the L-PBF fabrication, the heat transfer behavior of the powder bed differs from that of solids due to the partial contacts and inter-particle voids among the individual powder particles. Although the metal powder bed plays an important role in the heat transfer process, there has not existed a technique to measure the powder thermal properties directly. Numerical methods have been utilized by the authors to estimate the powder thermal conductivity in PBF AM [3]. The method utilizes finite element (FE) thermal modeling, which is also widely used in AM process simulations. FE modeling is critical in understanding the heat transfer process, predicting the optimal fabrication strategies and characterizing the fabricated parts in metal PBF. Gong *et al* [4] used FE model to obtain powder thermal conductivity by simulating the thermal field/history in the powder-bed election beam AM. Cheng *et al*

[5] and Zhang *et al* [3, 6] have recently developed a multivariable FE modeling approach to simulate the heat transfer process in the laser flash. This is combined with multi-point inverse optimization that uses the experimental results from laser flash, and eventually extracts the thermal properties of the powder.

Inputs of accurate material properties and process parameters in the FE simulation are important for the evaluation of the powder thermal properties. However, the uncertainties in the experiment and simulation processes are numerous. The sources of uncertainties are categorized into three types: the laser flash experiment, FE model, and the design of the hollow specimen fabricated in L-PBF. First, in the laser flash experiment, a flat cylindrical-shaped specimen receives a transient laser pulse of radiant energy on one side, and the thermal response is detected by an infrared (IR) pyrometer on the opposite side. The thermal diffusivity is then calculated from the sample thickness and the time required for the rising temperature to reach one-half of its maximum value. The estimated diffusivity is based on Parker's theory [7], which assumes one-dimensional heat transfer without heat losses and the tested specimen is homogeneous. Cezairliyan *et al* [8] reported the uncertainty with the thermal diffusivity caused by this assumption was estimated to be about 5% considering the heat loss effect. Subsequently, Ogawa *et al* [9] investigated the heat loss effect and reduced the uncertainty to under 0.4% by measuring a 3 mm thick alumina specimen at 1027 K. Another source of uncertainty in laser flash is that the IR pyrometer possibly delivers a baseline drift of the signal due to the electromagnetic disturbances induced by the laser pulse [10]. Additionally, Baba and Ono [11] pointed out that the laser irradiance on the sample is not spatially uniform enough to satisfy the ideal initial and boundary conditions whereby heat flows one-dimensionally in the specimen. They therefore investigated nonuniform energy distribution of the pulsed laser beam and developed the laser flash apparatus to decrease the nonuniform heating error by improving the laser beam using an optical fiber. Moreover, although the tested specimen is coated with dry graphite film to increase the energy absorption from the laser beam and the emission of the infrared radiation, the effect due to varying thickness of the coating is neglected [5].

Second, in order to accurately make the predictions, the thermal FE models require reliable material properties. Such material information is either obtained from reference literature or use reasonable assumptions [4, 12–15]. For example, the temperature-dependent material properties of solid titanium alloy Ti-6Al-4V (Ti64) used in the FE heat transfer model have an $\pm 10\%$ uncertainty of thermal conductivity and $\pm 3\%$ uncertainty of density [16]. In FE modeling research, it has been indicated that the specific heat and the latent heat of powder could be estimated to have the same values as the corresponding solid materials, due to the limited contribution of interstitial gas between powder particles [17–19]. In addition, different approaches used in the numerical simulation of the PBF process regard different sub-models to express the powder thermal properties. In the research of Körner *et al* [20] and Ammer *et al* [21], the models took the individual powder particles into account by a mesoscopic approach. On the other hand, in order to simplify the model and consequently to reduce large amount of calculation, the powder bed is defined as a continuum in some FE modeling work, such as that in [19]. The principal mechanism is to consider the powder bed with the pores between particles in a gaseous environment, and the effective thermal conductivity is based on the functional combination of the thermal conductivities of the solid and filling gas [17, 22, 23].

Third, the source of uncertainties is associated with the dimension of as-built parts in L-PBF. It has been investigated by some researchers that the dimensions of as-built parts by L-PBF rely on fabrication conditions and scan strategies. Van Bael *et al* found that the dimension of L-PBF Ti64 lattice structures was influenced by the geometries of the parts, and therefore, the pore shape and relative density were significantly varied [24]. Zhang *et al* [25, 26] and Yang *et al* [27] have investigated the effects of process parameters and scan strategies on the thin features in L-PBF, and found that the deposit with higher laser energy and which included contour scans would cause a larger offset to the as-built part.

It is challenging to confirm all uncertainties from experimental processes and simulations that are input into the FE model development. Much research work in engineering incorporates statistical analysis to speed up the design process and reduce the associated development costs. Various methods for design of experiment (DOE) have been utilized to optimize manufacturing processes extensively. For example, Ma *et al* [28] screened ten factors that may influence the part quality and minimized the simulation runs with a 2-level fractional factorial design to identify the critical variables. Shrestha and Manogharan [29] applied a Taguchi optimization method to determine the optimum AM parameters to improve transverse rupture strength in binder jetting processes. Likewise, the Taguchi method was revealed in numerous works [30–33] to identify critical variables through an orthogonal array-based DOE due to its straightforward and simple approach. In addition, the analysis of variance (ANOVA) method has been extensively reported. For instance, Zhang *et al* [34] adopted ANOVA to assist the analysis on tensile property variation based on different parameters and found additional correlations between the parameter factors and tensile outputs.

In this study, the major uncertainties were investigated in the measurement of metallic powder thermal properties in L-PBF. This includes analysis of the sensitivity of measured thermal properties to the specimen dimensions, thermal conductivity of solid material, irradiation region diameter, and pyrometer measured region diameter. These effects are subsequently demonstrated with the numerical-experimental approach combined with an FE heat transfer modeling and inverse method. Four major inputs in the FE model have been selected to investigate their sensitivity to the measurement. A statistical DOE approach was then adopted using a Taguchi method with dummy treatment, and the significance investigation and regression analysis were used to identify the critical variables for accurate measurements of the metallic powder thermal properties in L-PBF process.

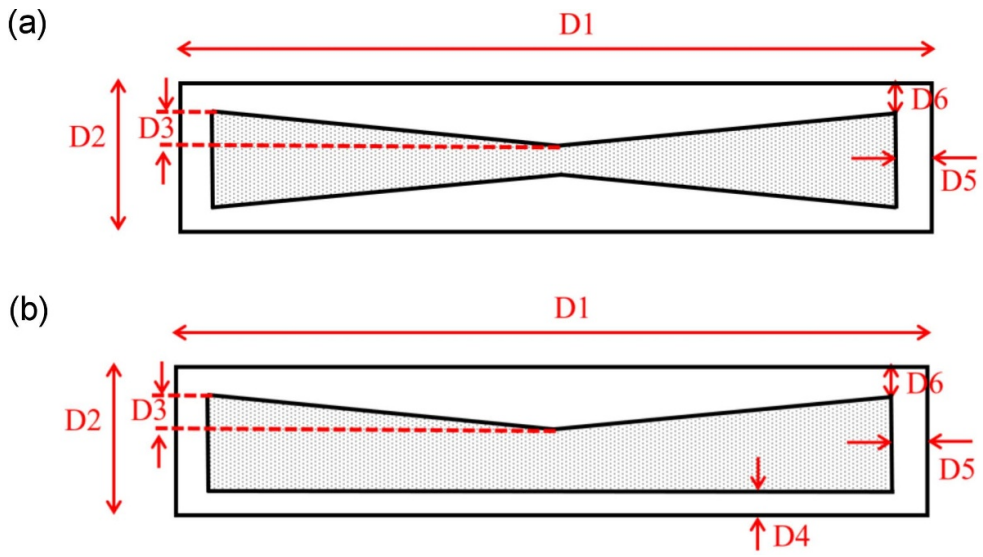

Figure 1. Illustration of dimension measurements of the powder-enclosed specimens with (a) double-conical feature (e.g.: 2Cone-0.5 and 2Cone-0.25) and (b) single-conical feature (e.g.: 1Cone-0.5). Note that the sketches do not reflect the dimensional ratio of actual specimens.

2. Methods

2.1. Experimental details

Similar to the studies of metallic powder-enclosed samples previously demonstrated [6], the experimental results were obtained from the laser flash apparatus using a sample size and shape with nomenclature 'D25mm Ti64 2Cone-0.5'. These flat, cylindrical Ti64 samples were vertically fabricated via L-PBF with a nominal external diameter of 25 mm, and internal conical features that were 0.5 mm thick, as seen in figures 1 and 2. As discussed in [6], the purpose of the conical features inside the hollow specimens was aimed to avoid a large-area gap caused by the powder settling, which may consequentially result in a heat transfer problem during laser flash. The same specimens were used for the sensitivity analysis purpose in this study. During measurement, the specimen is placed in the center of an alumina sample holder with a circular stand supporting it. The irradiation of the laser pulse in the laser flash process is assumed to have a uniform or 'top-hat' distribution, with an applied laser flux of 21.933 J s^{-1} mm^{-2} on the bottom side of the cylindrical specimen through a 22 mm opening. The pyrometer measures thermal response over a circular area on the top side of the specimen with approximate 10 mm diameter. Additionally, to better understand the measured dimension of the internal geometry, the specimens were sectioned through the center of the cylindrical sample, and then observed using optical microscopy for a fine measurement.

2.2. Numerical method

The inverse method combined with a heat transfer FE model that simulates the laser flash process is utilized in this study, which uses a powder-enclosed specimen design and is described in detail in previous studies by Cheng *et al* [5] and Zhang *et al* [3, 6]. The specimen and the alumina sample holder within the laser flash instrument were modeled with a mesh size of 0.5 mm and 0.7 mm, respectively. The following assumptions are set similar to the previous model: (a) The encapsulated powder together with the interstitial gas was treated as a continuum with designated homogenous powder thermal conductivity (k) and bulk density (ρ) as unknown variables. From the powder bulk density variable and known solid material density, powder porosity ($\Phi = 1 - \rho_{bulk}/\rho_{solid}$) can be calculated. The contact conductance between (a) the powder and the top shell (k_t), and (b) the powder and the bottom solid shell (k_b), are set as another two unknown variables. Additionally, the specimen-holder contact conductance (k_p) at testing temperatures used values obtained in the previous study.

Because of multiple unknowns, a multivariate inverse method with a multi-point optimization algorithm was utilized to fit the simulation results to the experimental results, and used to extract the powder thermal conductivity as one of the optimization variables through an iterative approach. The inverse approach uses the Levenberg–Marquardt method, which has been used in a variety of inverse heat transfer problems [35]. In this study, 20 points are selected on the experimental thermogram (i.e. measured temperature vs. time output from the laser flash apparatus), including 12 points in the heating period and 8 points in the cooling period, which are compared against the FE simulation data at the same time intervals. A sum-squared error (S) is calculated based on the difference between the measured thermogram and the FE simulation thermogram from the current iteration. For each iteration, a damping factor (u) is introduced to adjust the selection of optimal property variables for the next step iteration. The updated variable values, which include the unknown material thermal properties, are reincorporated in the FE model to perform the next iteration of the FE simulation and acquire another thermogram output. The S value is evaluated at each iteration to make sure that it is smaller than the previous iteration. If the current S value is larger than that in the previous iteration, the variables are calculated again from the

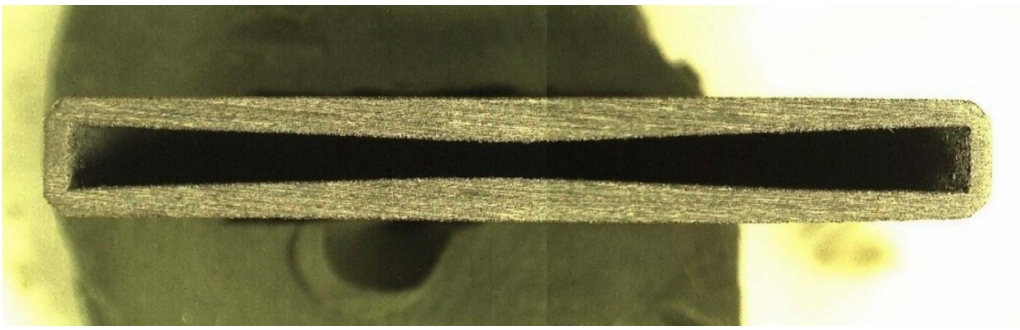

Figure 2. Radial cross-section of a 2Cone-0.5 Ti64 powder sample observed under a microscope.

previous iteration. When the S value is smaller than a user-defined criteria or cannot be further reduced, the iteration will stop and the result is considered optimal.

3. Effect of major uncertainties

In the powder property measurement process, including the L-PBF fabrication and laser flash analysis, there are plenty of factors that may influence the measurement. However, it is challenging and time-consuming to analyze the sensitivity of the measurement result to these parameters (e.g. through a full-factorial experiment design). It was noticed in the laser-flash specimens that there existed dimensional deviation between the designed geometry and measured geometry, where overall specimen thickness is a critical parameter in traditional laser flash analysis [7]. Also, thermal conductivity of solid material is applied for the solid shell of the powder-enclosed specimen as referred from literature [36]. In that study, a $\pm 10\%$ uncertainty of the nominal value induced non-negligible uncertainty. Furthermore, the input of accurate material parameters is critical for accurate predictions in the FE analysis. Therefore, four major uncertainties are analyzed in this section, and some preliminary findings are discussed.

3.1. Dimensions of the internal powder

The representative powder-enclosed specimens for the three cone configurations were radially sectioned along the diameter, and the dimensions were measured under an optical microscope. The measured dimensions of cone-featured specimens are marked as D1 to D6 in figure 1. An example of the radial cross-section of a 2Cone-0.5 sample was captured under a microscope, shown in figure 2. The dimensional measurements for three sample shapes (2Cone-0.5, 2Cone-0.25, and 1Cone-0.5) are shown in figure 3.

From the measurements of the Ti64 powder-enclosed specimens, it is noticed that the measured wall thickness (D5) is approximately 30% larger than design, and that the cone height difference (D3) varies between 8% and 13% while the external thickness (D2) are about 10% greater than designed. Such variation in dimension could be caused by the laser beam offset compensation and the measurement error due to roughness via L-PBF fabrication [37, 38].

To identify the dimension effect on the estimated powder thermal properties, the measured dimensions of Ti64 specimens were input into the FE heat transfer model in addition to the designed geometry, and the inverse numerical optimization algorithm applied to extract the corresponding thermal properties. The double-conical configuration (2Cone-0.5) of the Ti64 powder-enclosed specimens was investigated. Transient temperature is extracted from four nodal locations shown figure 4 for both the designed and measured sample geometry, with transient temperature results shown in figure 5.

From the comparison of temperature-time curves, it can be seen that the peak temperatures at points B, C, and D with the design dimension are higher than those with measured dimension input, while at point A, the comparison shows the opposite relationship, and the peak point occurs about 1 s later. For the latter, it is guessed that since the distance between the two cone tips is larger in the design-dimensioned model, the heat from the laser pulse traverses a longer path to the inner top surface where the laser-flash apparatus pyrometer would measure.

The measured dimension of the 2Cone-0.5 Ti64 specimen was input into the FE models at 100 °C–500 °C to analyze the powder thermal conductivity and density. In these models, the coefficient of thermal expansion of Ti64 at different temperatures is taken into account, as shown in figure 6.

The powder thermal conductivity at various temperatures was analyzed using the inverse method and the results are summarized in figure 7. Generally, the thermal conductivity still maintains an increasing linear trend with a high fitting R^2 value, although the measured dimensions lead to a slightly higher thermal conductivity. Besides, it is noted that the thermal conductivity ratio of the powder is consistently about 5% relative to the solid counterpart regardless of the temperature [6]. On the other hand, the powder porosity remains in a range from 44.3% to 50%, with a minor difference between design and measured dimensions (figure 8). From the comparison between different dimensions in figure 8, it is also noticed that the range that the powder porosity extracted from the inverse method dimensions is slightly lower when using the measured dimensions compared to that using the design dimensions.

Similar to the 2Cone-0.5 Ti64 specimen, the measured dimensions of the 1Cone-0.5 powder-enclosed specimen are

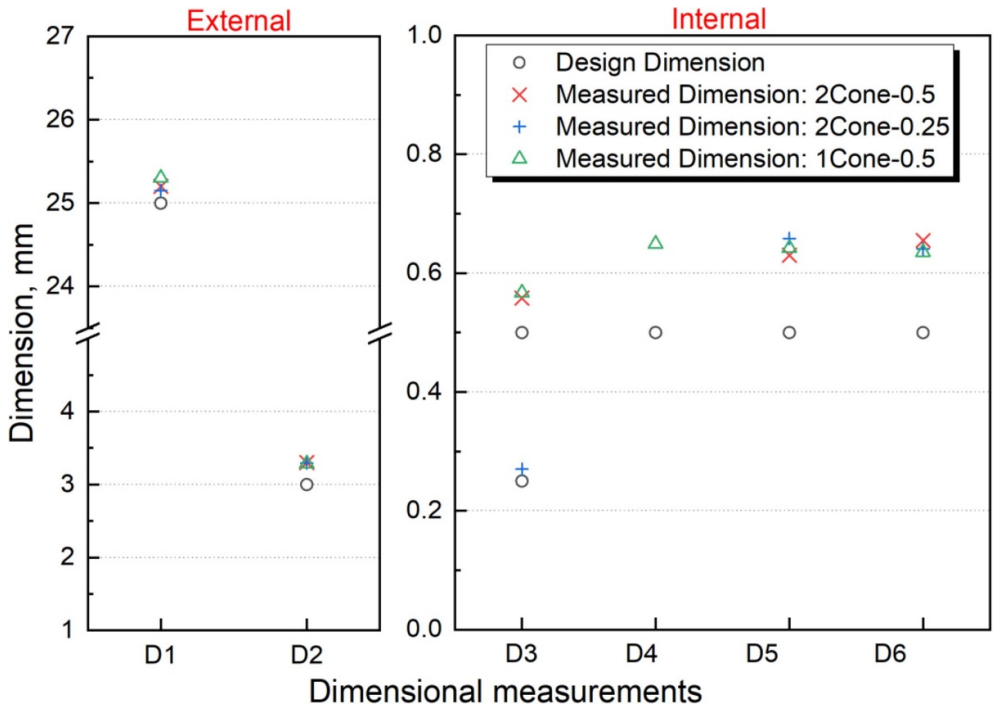

Figure 3. Dimensional measurements with three different conical featured specimens.

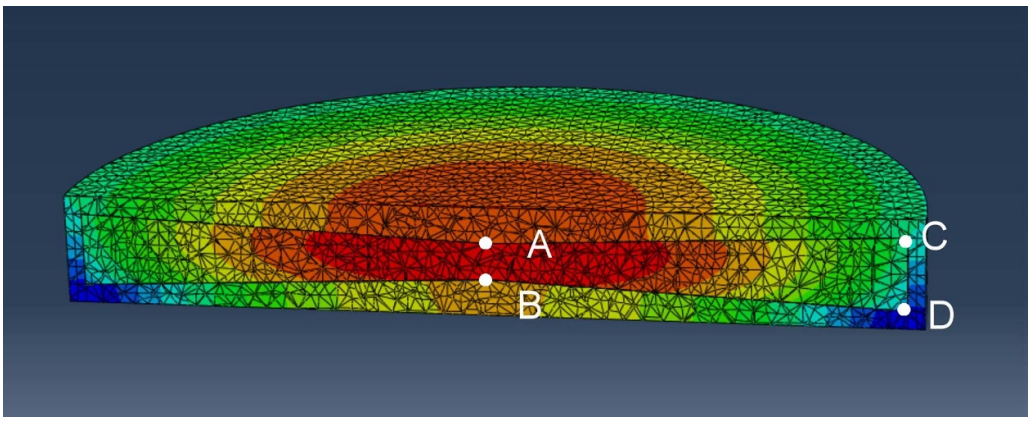

Figure 4. 2Cone-0.5 Ti64 specimen in simulation at 100 °C, points taken on powder.

also input into the FE model to estimate the powder thermal properties at the tested temperatures using the inverse method. It is observed in figure 9 that the powder thermal conductivity has a highly linear trend despite an overall decrease of the powder thermal conductivity ratio to the solid (approximately 3.6%). The porosity at various temperatures is noted and shown to be within the range of 47.9%–52.8% for the measured dimension, which is about 1.85% lower than that from the design dimensions (figure 10).

3.2. Thermal conductivity of the solid Ti64 material

According to the referred thermal conductivity of solid Ti64 material in figure 11, a ±10% uncertainty in the tabulated values is provided, and therefore, will result in uncertainty in powder thermal conductivity determined from the simulation-based inverse method described in this work. To investigate the effect of this uncertainty, the powder thermal properties were analyzed using the inverse method incorporating a ±10% of the average thermal conductivity of solid Ti64 at 100 °C in the FE simulation. The 2Cone-0.5 powder specimen was used for this purpose.

The analytical results for the 2Cone-0.5 Ti64 specimen with ±10% of the average thermal conductivity at 100 °C are summarized in figure 12. It is observed that the extracted powder thermal conductivity is about 5% higher when applying a 10% lower solid thermal conductivity into the FE model, while it is 3% lower with a 10% upper conductivity input. On the other hand, the powder density increases no matter how the solid thermal conductivity changes, and the powder density varies within approximately 5% (figure 12).

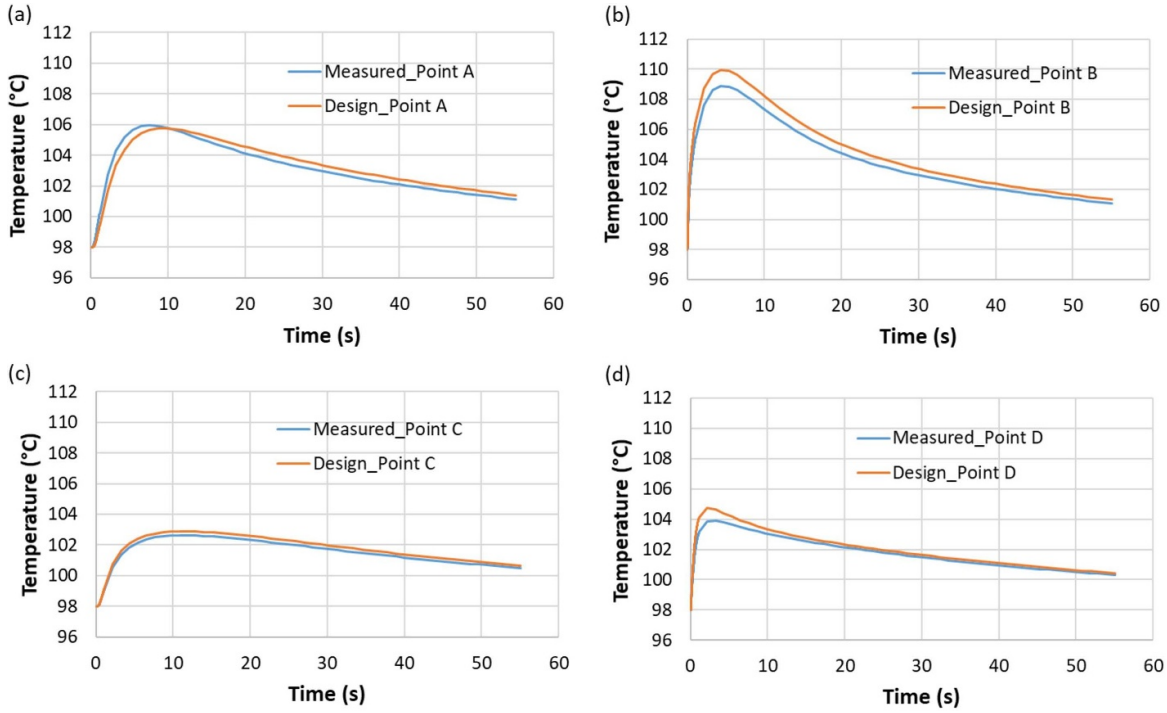

Figure 5. Comparison of temperature-time curves between design dimension and measured dimension at points A, B, C, and D, at 100 °C.

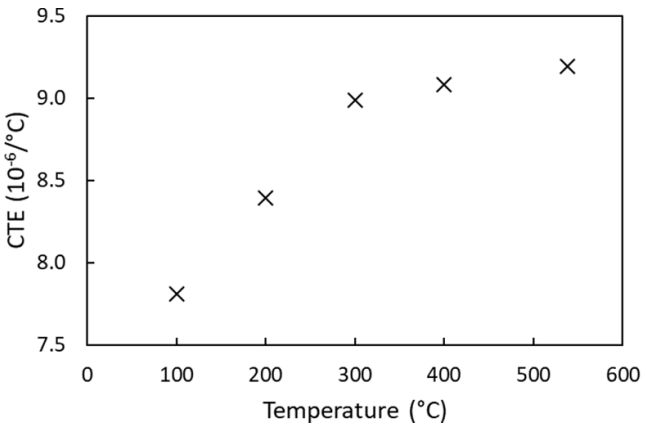

Figure 6. Coefficient of thermal expansion for Ti64 [39].

Figure 13 shows a comparison of thermograms among the three cases. At the heating period, the curve exhibits a higher slope when using a 10% higher solid Ti64 conductivity in the model, while the curve with a 10% lower values is close to the original. On the other hand, the plots using ±10% solid Ti64 thermal conductivity at the cooling period are distributed on both sides of the original, respectively.

3.3. Irradiation area

Since the specimen is sitting on a circular stand of the sample holder, the irradiation area cannot be expanded larger than the diameter of 22 mm. To check the effect of the irradiation area on the powder thermal property measurement, a 5% reduced diameter is input into the FE model and the resultant powder thermal properties are compared. Under the same conditions in the FE model except for different irradiation diameter, the comparison of optimization parameter S values exhibit little difference, showing 0.001204 and 0.001206 respectively. The non-significant change is also verified from the comparison between the two thermograms in figure 14.

3.4. Detected area

Another uncertain parameter from the laser flash experiment is the detected area on the top side of the specimen measured by the pyrometer. The nominal diameter for the heat response detection from the pyrometer is 10 mm. To investigate the influence of the detected area on the analytical results of the powder thermal properties, ±5% variation of the diameter of the detected area is conducted in simulation. The results are compared with that using the original diameter of 10 mm. The compared thermograms between different detected areas are shown in figure 15, indicating insignificant dependence on the detector area.

4. Statistical sensitivity analysis

Based on the preliminary findings, it is noticed that the specimen dimension and solid material thermal conductivity influence the evaluation of the powder thermal properties. Although the irradiation area and detected area were not observed to have significant influence, their significance degree can be statistically different, which may lead to non-neglected weights in regression analysis. Therefore, the four critical uncertain variables were all included to analyze their sensitivity to the powder thermal properties in L-PBF. In

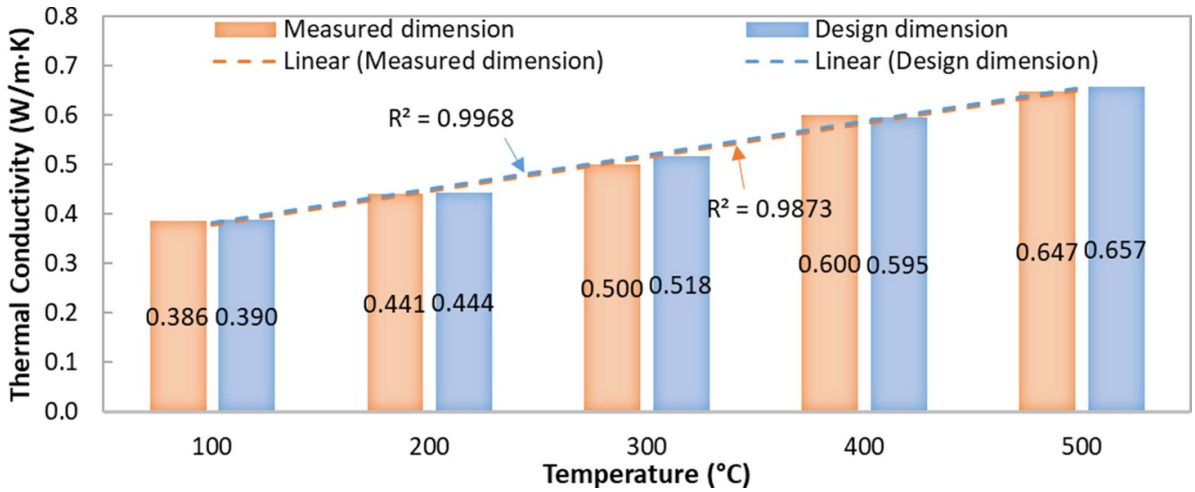

Figure 7. Comparison of powder thermal conductivity from 2Cone-0.5 Ti64 specimen between using design dimension and measured dimension at different temperatures.

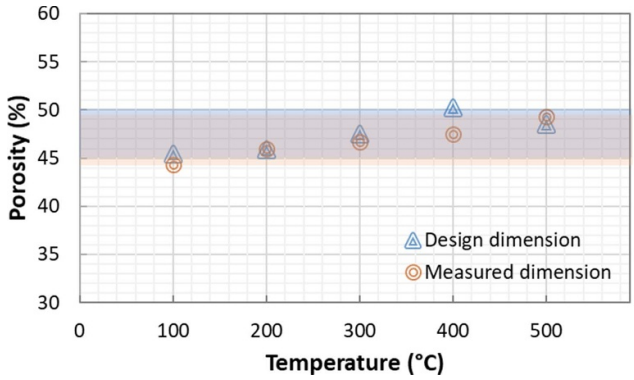

Figure 8. Comparison of powder porosity from 2Cone-0.5 Ti64 specimen between using design dimension and measured dimension at different temperatures. Overlay bands indicate the range of values for the design or measured dimension datasets.

this study. a statistical DOE method was utilized. A dummy-treated Taguchi method was used to design the factor combinations. The ANOVA method was adopted to analyze the main factor effects and significance to the response. Then, the regression analysis was conducted to estimate the correlations between the factors and response, followed by a validation of a case study.

4.1. DOEs

Due to the consideration of time and computational source occupied, a Taguchi design approach was adopted in the sensitivity investigation. Four major variables at 100 °C were selected based on the above work, including the coefficients of biases for dimension (X1), thermal conductivity of the solid Ti64 (X2), irradiation region diameter (X3), and pyrometer measured region diameter (X4). An L27 (3^4) orthogonal array with dummy treatment was carried out in this study, as shown in table 1. This array included three levels for each control factor to detect the effects of the interactions of parameters. Additionally, the dummy treatment allowed for the factor X3 at two levels expanding into three, while maintaining the orthogonality by repeating one of the only two levels [40].

4.2. Results and discussion

The FE heat transfer model was then updated using the 27 combinations of factor levels in table 1, and the inverse method was utilized to measure the powder thermal properties for each corresponding condition accordingly. The analytical results were estimated and summarized in table 2. The resultant powder thermal conductivity (k) and porosity (Φ) were investigated based on the influences of the factors and analyzed statistically using ANOVA and regression analysis.

4.2.1. Main effect The main effect plots for powder thermal conductivity and porosity are graphed to indicate the mean values of powder thermal conductivity and porosity at each level of the four factors directly, shown in figure 16. It can be observed that different factors and different levels affect the responses differently. X1 and X2 seem to affect the powder thermal conductivity more obviously because the plots cross the mean values of the thermal conductivity wider. Also, as X1 and X2 increase levels, the thermal conductivity a decreases linearly. For X3, there is no distinct effect on the powder thermal conductivity demonstrated by a nearly horizontal plot. The lower level of X4 leads to a higher powder thermal conductivity, with the 0 level staying in between. On the other hand, the plot between X1 = 0 and X1 = 0.3 shows a steep slope, which indicates the main effect of higher level of X1 (dimension) has greater influence to the thermal conductivity and powder porosity, although the entire plot shows a decreasing trend as X1 increases. In addition, X2 (solid thermal conductivity) and X4 (pyrometer measured region diameter) result in an opposite effect to the powder porosity, while X3 (irradiation region diameter) shows no obvious effect.

4.2.2. ANOVA The main effect plots show a pattern how the four factors affect the mean values of the powder

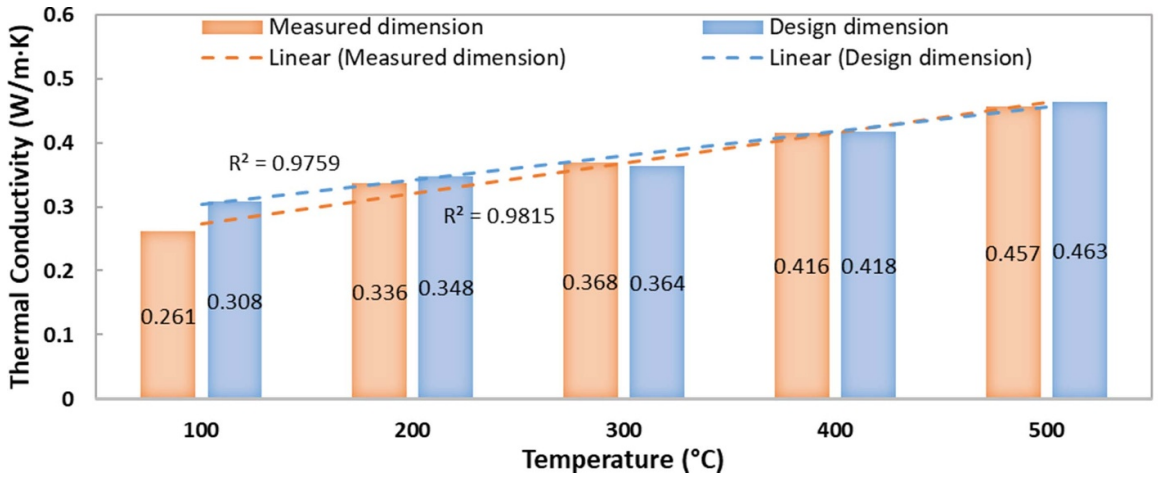

Figure 9. Comparison of powder thermal conductivity from 1Cone-0.5 Ti64 specimen between using design dimension and measured dimension at different temperatures.

Table 1. Dummy-treated L27 Taguchi design at 100 °C.

	Run #	*1*	*2*	*3*	*4*	*5*	*6*	*7*	*8*	*9*
X1[a]		0.3	0.3	0.3	0	0	0	−0.3	−0.3	−0.3
X2		0.1	0	−0.1	0.1	0	−0.1	0.1	0	−0.1
X3		0	0	0	0	0	0	0	0	0
X4		0.05	0	−0.05	0	−0.05	0.05	−0.05	0.05	0
	Run #	*10*	*11*	*12*	*13*	*14*	*15*	*16*	*17*	*18*
X1		0.3	0.3	0.3	0	0	0	−0.3	−0.3	−0.3
X2		0.1	0	−0.1	0.1	0	−0.1	0.1	0	−0.1
X3		−0.05	−0.05	−0.05	−0.05	−0.05	−0.05	−0.05	−0.05	−0.05
X4		0.05	0	−0.05	0	−0.05	0.05	−0.05	0.05	0
	Run #	*19*	*20*	*21*	*22*	*23*	*24*	*25*	*26*	*27*
X1		0.3	0.3	0.3	0	0	0	−0.3	−0.3	−0.3
X2		0.1	0	−0.1	0.1	0	−0.1	0.1	0	−0.1
X3		0	0	0	0	0	0	0	0	0
X4		0	−0.05	0.05	−0.05	0.05	0	0.05	0	−0.05

[a] Coefficients of biases (dimensionless unit) for the four parameters.

Table 2. Analytical results using the inverse method based on the design in table 1.

	Run #	*1*	*2*	*3*	*4*	*5*	*6*	*7*	*8*	*9*
k, W m^{-1} K^{-1}		0.351	0.382	0.406	0.384	0.420	0.418	0.406	0.417	0.425
Φ, %		40.73	41.65	41.07	44.68	43.00	47.22	43.80	44.08	45.13
	Run #	*10*	*11*	*12*	*13*	*14*	*15*	*16*	*17*	*18*
k, W m^{-1} K^{-1}		0.357	0.381	0.399	0.389	0.415	0.416	0.398	0.410	0.413
Φ, %		40.68	41.70	39.49	42.74	43.87	47.34	45.13	45.27	47.03
	Run #	*19*	*20*	*21*	*22*	*23*	*24*	*25*	*26*	*27*
k, W m^{-1} K^{-1}		0.353	0.381	0.398	0.392	0.392	0.428	0.394	0.411	0.421
Φ, %		41.03	42.72	44.64	44.04	47.24	45.33	45.14	45.48	45.93

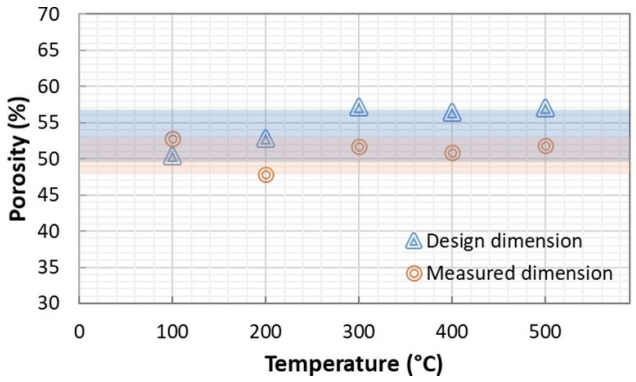

Figure 10. Comparison of powder porosity from 1Cone-0.5 Ti64 specimen between using design dimension and measured dimension at different temperatures. Overlay bands indicate the range of values for the design or measured dimension datasets.

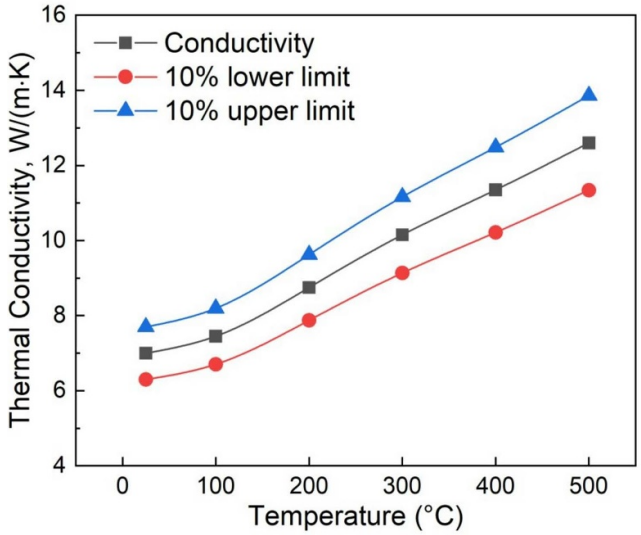

Figure 11. Solid Ti64 thermal conductivity [36].

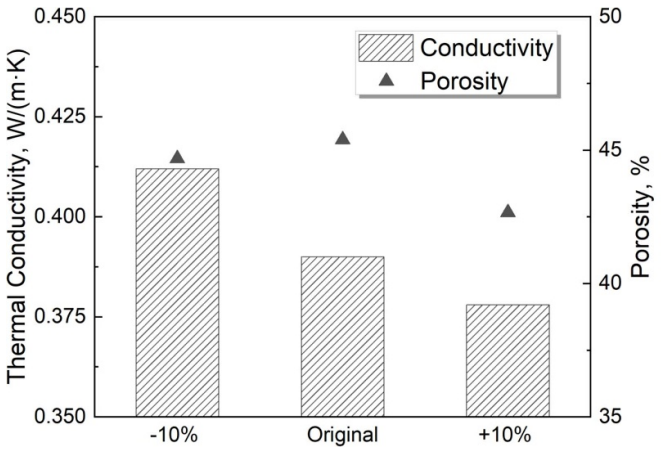

Figure 12. Comparison of extracted powder thermal conductivity and porosity when applying a ±10% change in solid material thermal conductivity to the FE model.

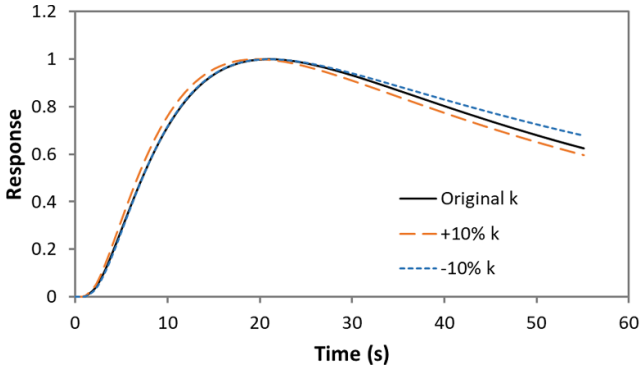

Figure 13. Comparison of thermograms between the nominal solid Ti64 thermal conductivity and when applying ±10% of the nominal value (at a sample/environment temperature of 100 °C).

thermal conductivity and porosity. However, to determine the significance of each factor, the ANOVA is necessary. A general linear model (GLM) is utilized to determine the significance of the four factors with a confidence interval of 95% in this case. In GLM, the calculations are performed using a least squares regression approach to evaluate the statistical relationship between one or more factors and the continuous responses. Table 3 exhibits the significance investigation from the ANOVA statistical analysis on the four main factors of X1–X4 and their 2nd-order interactions to the powder thermal conductivity and porosity, respectively. The corresponding R squared values are 99.45% and 93.94%.

From table 3, it is noticed that the P-values for X1 and X2 as well as their interaction are less than 0.05, which interpret that X1 and X2 are significant factors to the powder thermal conductivity. Because of their P-values larger than 0.05, other factors are non-significant. Additionally, the P-values for the second order interactions of the four factors are greater than 0.05, indicating no interaction is significant to the powder conductivity. On the other hand, only X1 is seen as a significant factor to the powder porosity while others are not significant.

4.2.3. Regression analysis Then, a regression analysis is adopted to estimate the relationship between the factors and the responses, and therefore widely used for prediction by the resultant regression equations. The regression analysis was performed in this work to investigate the relationship between X1 and X4 and dependent outputs of powder thermal conductivity and porosity. A fit regression model was utilized and regression equations generated for a further prediction.

For the powder thermal conductivity (k), the linear and nonlinear equations were first attempted, as shown in equations (1) and (2), respectively. The corresponding R^2 for both statistical models are 0.9158 and 0.9222, indicating the nonlinear equation is slightly more reliable. Another attempt was to use the Box–Cox transformation [41], and the coefficients of λ and g were introduced, as shown in equation (3). This equation shows a higher R^2 of 0.9808, which is considered a

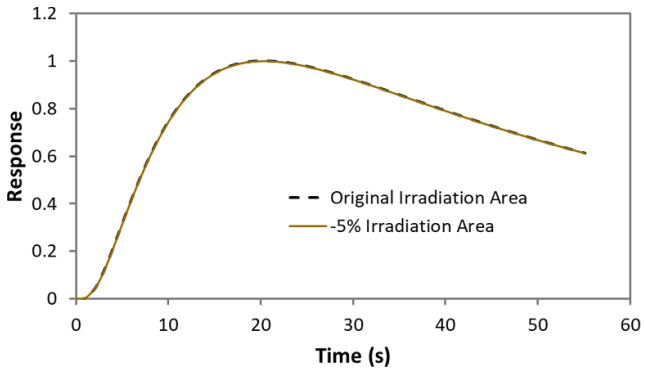

Figure 14. Comparison of simulated thermograms resulting from two different irradiation areas.

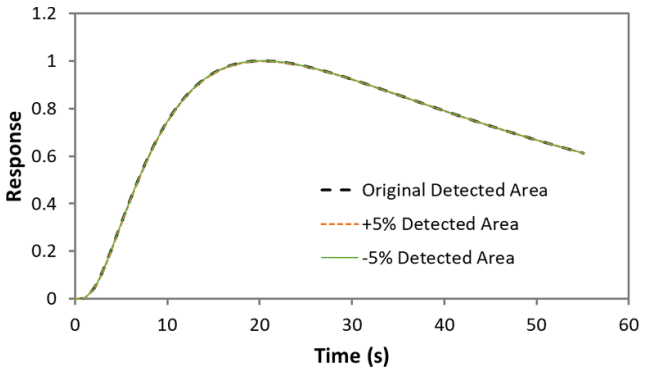

Figure 15. Simulated thermogram results comparing different detector areas.

more desirable reliability and will be used for analysis for the next step.

$$k = 0.39892 - 0.05675X1 - 0.1818X2 + 0.0294X3 - 0.0936X4 - 0.1245X1 \times X2 - 0.378X1 \times X3 - 0.249X1 \times X4 - 1.245X2 \times X3 - 1.110X2 \times X4 - 0.73X3 \times X4 \quad (1)$$

$$-k^{-0.5} = -1.58520 - 0.1167X1 - 0.3699X2 + 0.046X3 - 0.1978X4 - 0.313X1 \times X2 - 0.779X1 \times X3 - 0.554X1 \times X4 - 2.55X2 \times X3 - 2.38X2 \times X4 - 1.56X3 \times X4 \quad (2)$$

$$(k^{\lambda-1}) \Big/ (\lambda \times g^{\lambda-1}) = -0.08723 - 0.06438X1 - 0.1996X2 + 0.0084X3 - 0.1169X4 - 0.1369X1 \times X1 - 0.503X2 \times X2 - 0.315X4 \times X4 - 0.3396X1 \times X2 - 0.262X1 \times X3 - 0.111X1 \times X4 - 1.050X2 \times X3 - 0.362X2 \times X4 - 1.54X3 \times X4 \quad (3)$$

where $\lambda = -4$ and $g = 0.397857$ is the geometric mean of k.

Likewise, a regression analysis for powder porosity was carried out to examine the relationship with the four factors. Equation (4) shows the linear functions that include all four main factors and their 2nd-order interactions, followed by a R^2 of 0.795. When taking the squared factor terms into account, the regression provides an updated equation, as shown in equation (5). It is noted that since X3 is the least significant term from ANOVA, the squared X3 is not put into the equation. Then this equation gives a higher R^2 of 0.8714. In addition, a non-linear equation was attempted with all feasible 1st- and 2nd order terms as shown in equation (6), and the R^2 is 0.8737.

$$\rho = 0.44051 - 0.0492X1 - 0.0825X2 + 0.071X3 + 0.1415X4 + 0.045X1 \times X2 + 0.392X1 \times X3 + 0.141X1 \times X4 + 0.33X2 \times X3 - 2.118X2 \times X4 - 0.10X3 \times X4 \quad (4)$$

$$\rho = 0.45073 - 0.0492X1 - 0.0825X2 + 0.0712X3 + 0.1415X4 - 0.1579X1 \times X1 - 0.176X2 \times X2 + 0.25X4 \times X4 - 0.027X1 \times X2 + 0.573X1 \times X3 + 0.318X1 \times X4 + 0.60X2 \times X3 - 1.031X2 \times X4 - 0.53X3 \times X4 \quad (5)$$

$$\ln(\rho) = -0.7967 - 0.1139X1 - 0.1867X2 + 0.178X3 + 0.314X4 - 0.361X1 \times X1 - 0.47X2 \times X2 + 0.38X4 \times X4 - 0.070X1 \times X2 + 1.324X1 \times X3 + 0.725X1 \times X4 + 1.14X2 \times X3 - 2.43X2 \times X4 - 1.40X3 \times X4 \quad (6)$$

4.2.4. Case study Based on the equation reliability, equations (3) and (6) are the optimal prediction for the powder thermal conductivity and porosity with the range of tested factors in this study. To investigate the prediction accuracy, a case study section is conducted for verification purpose. Two groups of randomly generated values within the investigated ranges of X1, X2, X3, and X4 are shown in table 4. Based on the variations in each case, the corresponding parameters were input into the FE model for performing the powder thermal conductivity and porosity estimation via the inverse method.

Through the inverse procedure using FE modeling, the analytical results for both cases are exhibited in table 5. In addition, the predicted powder thermal conductivity and porosity results are also calculated using equations (3) and (6), respectively, and then compared with the analytical results.

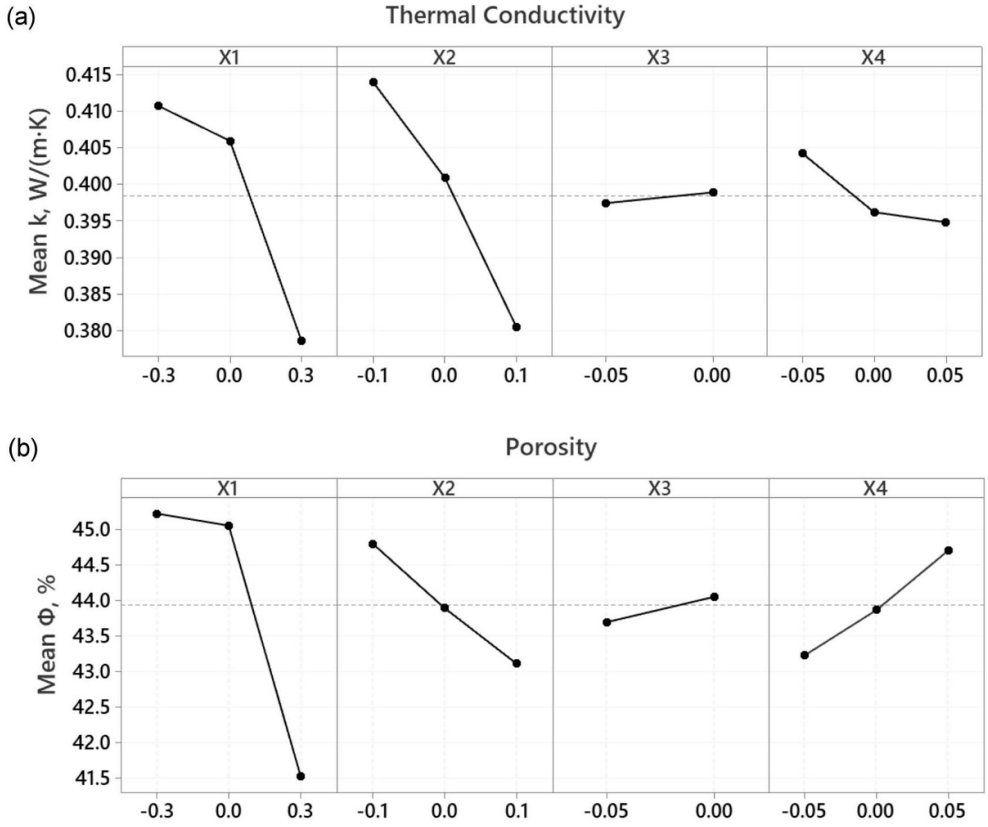

Figure 16. Main effect plots for (a) thermal conductivity and (b) porosity of Ti64 powder.

Table 3. Significance investigation on the powder thermal conductivity and porosity and 2nd-order interactions evaluated at 100 °C.

	P-value	
Source	*k*	*Φ*
X1	0.000	0.003
X2	0.000	0.296
X3	0.919	0.802
X4	0.132	0.115
X1 × X2	0.004	0.827
X1 × X3	0.343	0.299
X1 × X4	0.177	0.318
X2 × X3	0.215	0.806
X3 × X4	0.355	0.986
R^2	99.45%	93.94%

Table 4. Randomly generated properties for two cases.

	Case 1	Case 2
X1	−0.10	0.17
X2	−0.04	−0.02
X3	−0.04	−0.01
X4	0.00	−0.04

It can be observed that the powder thermal conductivity and porosity through FE simulation and the inverse method do not significantly differ from the analytical regression equations.

Table 5. Comparison between the prediction and analytical results in cases 1 and 2.

		Simulation	Analytical	Difference
Case 1	k, W m^{-1} K^{-1}	0.418	0.410	1.74%
	Φ, %	45.70	46.89	2.61%
Case 2	k, W m^{-1} K^{-1}	0.403	0.401	0.46%
	Φ, %	43.02	44.17	2.66%

The differences between the predicted and analytical properties are less than 3%, and therefore, verify the reasonability of the regression equations.

5. Conclusions

This study is focused on the sensitivity analysis of the uncertainties in the FE model and laser flash experiment process. First, the preliminary examinations investigated four major uncertainties, including the dimensions of the powder-encapsulated volume, solid Ti64 thermal conductivity, and the irradiation area and pyrometer detected area from the laser flash. It was found that the internal powder dimension and the solid material properties resulted in a noticeable difference in the thermograms and analytical values, while the other two variables did not cause obvious differences based on the tested properties. Particularly, the measured dimensions led to a slightly more linear trend in the thermal conductivity of the

powder, ranging from 0.26 W m^{-1} K^{-1} to 0.65 W m^{-1} K^{-1}. On the other hand, the porosity remains in the range of 44%–52% across different temperatures, but compared to the results using the design dimensions, the powder porosity using the measured dimension stays in a narrower range.

In addition, the sensitivity of the four factors to the powder thermal properties in L-PBF was evaluated. A Taguchi method with dummy treatment was utilized to design the experiments. Then the corresponding FE models were set up with the respective factors at varying levels, and the inverse method was conducted to determine the powder thermal conductivity and porosity. The results showed the significance of the factors and their interactions using ANOVA. The relationship between the factors and responses was predicted using the regression analysis. The major findings are concluded as follows.

(a) Within the tested temperature range, the internal dimension and solid material thermal conductivity appear to significantly affect the extracted powder thermal conductivity value, while the irradiation area and detected area do not exhibit significant contribution.
(b) The internal dimension has a significant influence on the extracted porosity values of the powder.
(c) The interaction of the internal dimension and solid thermal conductivity significantly affects the extracted powder thermal conductivity. Yet, none of the interactions of the four factors significantly affect the extracted powder porosity.
(d) The Box–Cox transformed non-linear regression equation (equation (3)) exhibits an optimal prediction to the powder thermal conductivity and a non-linear equation considering 2nd-order terms (equation (6)), gives an optimal prediction to the porosity in this study. The two prediction equations were then verified using the FE modeling and the inverse method with a good agreement.

Acknowledgments

This study is supported by NIST (CA No. 70NANB16H029). The authors also acknowledge the technical support from the Rapid Prototyping Center and the computational resources from the Cardinal Research Cluster at University of Louisville.

ORCID iD

Shanshan Zhang https://orcid.org/0000-0003-1023-8293

References

[1] Gokuldoss P K, Kolla S and Eckert J 2017 Additive manufacturing processes: selective laser melting, electron beam melting and binder jetting—selection guidelines *Materials* **10** 672
[2] Gibson I, Rosen D and Stucker B 2015 Directed energy deposition processes *Additive Manufacturing Technologies* (Berlin: Springer) pp 245–68
[3] Zhang S, Lane B M, Whiting J G and Chou K 2018 An investigation into metallic powder thermal conductivity in laser powder bed fusion additive manufacturing *Solid Freeform Fabrication Symp.*
[4] Gong X, Cheng B, Price S and Chou K 2013 Powder-bed electron-beam-melting additive manufacturing: powder characterization, process simulation and metrology *Proc. ASME District F Early Career Technical Conf.*
[5] Cheng B, Lane B, Whiting J and Chou K 2018 A combined experimental-numerical method to evaluate powder thermal properties in laser powder bed fusion *J. Manuf. Sci. Eng.* **140** 111008
[6] Zhang S, Lane B, Whiting J and Chou K 2019 On thermal properties of metallic powder in laser powder bed fusion additive manufacturing *J. Manuf. Process.* **47** 382–92
[7] Parker W J, Jenkins R J, Butler C P and Abbott G L 1961 Flash method of determining thermal diffusivity, heat capacity, and thermal conductivity *J. Appl. Phys.* **32** 1679–84
[8] Cezairliyan A, Baba T and Taylor R 1994 A high-temperature laser-pulse thermal diffusivity apparatus *Int. J. Thermophys.* **15** 317–41
[9] Ogawa M, Mukai K, Fukui T and Baba T 2001 The development of a thermal diffusivity reference material using alumina *Meas. Sci. Technol.* **12** 2058
[10] Hay B, Filtz J R, Hameury J and Rongione L 2005 Uncertainty of thermal diffusivity measurements by laser flash method *Int. J. Thermophys.* **26** 1883–98
[11] Baba T and Ono A 2001 Improvement of the laser flash method to reduce uncertainty in thermal diffusivity measurements *Meas. Sci. Technol.* **12** 2046
[12] Shrestha S, Rauniyar S and Chou K 2019 Thermo-fluid modeling of selective laser melting: single-track formation incorporating metallic powder *J. Mater. Eng. Perform.* **28** 611–9
[13] Bikas H, Stavropoulos P and Chryssolouris G 2016 Additive manufacturing methods and modelling approaches: a critical review *Int. J. Adv. Manuf. Technol.* **83** 389–405
[14] Zeng K, Pal D and Stucker B 2012 A review of thermal analysis methods in laser sintering and selective laser melting *Proc. Solid Freeform Fabrication Symp.* (*Austin, TX*)
[15] Galati M, Iuliano L, Salmi A and Atzeni E 2017 Modelling energy source and powder properties for the development of a thermal FE model of the EBM additive manufacturing process *Addit. Manuf.* **14** 49–59
[16] Mills K C 2002 *Recommended Values of Thermophysical Properties for Selected Commercial Alloys* (Cambridge: Woodhead Publishing)
[17] Tolochko N K, Arshinov M K, Gusarov A V, Titov V I, Laoui T and Froyen L 2003 Mechanisms of selective laser sintering and heat transfer in Ti powder *Rapid Prototyp. J.* **9** 314–26
[18] Shen N and Chou K 2012 Thermal modeling of electron beam additive manufacturing process: powder sintering effects *ASME 2012 Int. Manufacturing Science and Engineering Conf. Collocated with the 40th North American Manufacturing Research Conf. and in Participation with the Int. Conf. on Tribology Materials and Processing* (American Society of Mechanical Engineers)
[19] Zäh M F and Lutzmann S 2010 Modelling and simulation of electron beam melting *Prod. Eng.* **4** 15–23
[20] Körner C, Attar E and Heinl P 2011 Mesoscopic simulation of selective beam melting processes *J. Mater. Process. Technol.* **211** 978–87
[21] Ammer R, Rüde U, Markl M and Körner C 2017 *Modeling of Thermodynamic Phenomena with Lattice Boltzmann Method for Additive Manufacturing Processes*
[22] Roberts I A, Wang C J, Esterlein R, Stanford M and Mynors D J 2009 A three-dimensional finite element analysis of the temperature field during laser melting of

metal powders in additive layer manufacturing *Int. J. Mach. Tools Manuf.* **49** 916–23
[23] Bugeda Miguel Cervera G and Lombera G 1999 Numerical prediction of temperature and density distributions in selective laser sintering processes *Rapid Prototyp. J.* **5** 21–26
[24] Van Bael S, Chai Y C, Truscello S, Moesen M, Kerckhofs G, Van Oosterwyck H, Kruth J-P and Schrooten J 2012 The effect of pore geometry on the *in vitro* biological behavior of human periosteum-derived cells seeded on selective laser-melted Ti6Al4V bone scaffolds *Acta Biomater.* **8** 2824–34
[25] Zhang S 2017 *Design, Analysis, and Application of a Cellular Material/Structure Model for Metal Based Additive Manufacturing Process*
[26] Zhang S, Dilip S, Yang L, Miyanaji H and Stucker B 2015 Property evaluation of metal cellular strut structures via powder bed fusion AM *Proc. Solid Freeform Fabrication (SFF) Symp.* (*Austin, TX, USA*)
[27] Yang L, Harrysson O, Cormier D, West H, Gong H and Stucker B 2015 Additive manufacturing of metal cellular structures: design and fabrication *JOM* **67** 608–15
[28] Ma L, Fong J, Lane B, Moylan S, Filliben J, Heckert A and Levine L 2015 Using design of experiments in finite element modeling to identify critical variables for laser powder bed fusion *Int. Solid Freeform Fabrication Symp.* (*Austin, TX*: Laboratory for Freeform Fabrication and the University of Texas)
[29] Shrestha S and Manogharan G 2017 Optimization of binder jetting using Taguchi method *JOM* **69** 491–7
[30] Lakshmi K S and Arumaikkannu G 2014 Influence of process parameters on surface finish in customized bone implant using selective laser sintering *Adva. Mater. Res.* **845** 862–7
[31] Jiang H-Z, Li Z-Y, Feng T, Wu P-Y, Chen Q-S, Feng Y-L, Li S-W, Gao H and Xu H-J 2019 Factor analysis of selective laser melting process parameters with normalised quantities and Taguchi method *Opt. Laser Technol.* **119** 105592
[32] Sun J, Yang Y and Wang D 2013 Parametric optimization of selective laser melting for forming Ti6Al4V samples by Taguchi method *Opt. Laser Technol.* **49** 118–24
[33] Asgari G, Dayari A, Ghasemi M, Seid-Mohammadi A, Gupta V K and Agarwal S 2019 Efficient fluoride removal by preparation, characterization of pyrolysis bone: mixed level design experiment and Taguchi L8 orthogonal array optimization *J. Mol. Liq.* **275** 251–64
[34] Zhang S, Rauniyar S, Shrestha S, Ward A and Chou K 2019 An experimental study of tensile property variability in selective laser melting *J. Manuf. Process.* **43** 26–35
[35] Ozisik M N 2000 *Inverse Heat Transfer: Fundamentals and Applications* (Boca Raton, FL: CRC Press)
[36] Yang J, Sun S, Brandt M and Yan W 2010 Experimental investigation and 3D finite element prediction of the heat affected zone during laser assisted machining of Ti6Al4V alloy *J. Mater. Process. Technol.* **210** 2215–22
[37] Yang L, Gong H, Dilip S and Stucker B 2014 An investigation of thin feature generation in direct metal laser sintering systems *Solid Freeform Fabrication Symp.*
[38] Mumtaz K and Hopkinson N 2009 Top surface and side roughness of inconel 625 parts processed using selective laser melting *Rapid Prototyp. J.* **15** 96–103
[39] Characterizing the Coefficient of Thermal Expansion of a Medical Grade (available at: https://ctherm.com/resources/blog/characterizing_the_cte_coefficient_of_thermal_expansion_of_a_medical_grade/)
[40] Ross P J and Ross P J 1988 *Taguchi Techniques for Quality Engineering: Loss Function, Orthogonal Experiments, Parameter and Tolerance Design* (New York: McGraw-Hill)
[41] Box G E P and Cox D R 1964 An analysis of transformations *J. R. Stat. Soc.* B **26** 211–43